ELSEVIER

Journal of Alloys and Compounds 404–406 (2005) 413–416

Journal of ALLOYS AND COMPOUNDS

www.elsevier.com/locate/jallcom

Hydrogen sorption properties of Mg–1 wt.% Ni–0.2 wt.% Pd prepared by reactive milling

O. Gutfleisch[a,*], S. Dal Toè[a], M. Herrich[a], A. Handstein[a], A. Pratt[b]

[a] *IFW Dresden, Institut für Metallische Werkstoffe, Helmholtzstr. 20, D01069 Dresden, Germany*
[b] *Johnson Matthey Technology Centre, Reading RG4 9NH, UK*

Received 31 May 2004; received in revised form 20 September 2004; accepted 27 September 2004
Available online 11 July 2005

Abstract

Despite the large differences in melting points and the high vapour pressure of Mg, we succeeded in the preparation of induction-melted Mg–1 wt.% Ni–0.2 wt.% Pd alloy. The alloy was then reactively ball milled in 10 bar hydrogen. The structural changes during milling were characterised by XRD and high resolution scanning electron microscopy. The hydrogen sorption properties have been systematically studied by gravimetric analysis in a wide temperature and pressure range for absorption (1–10 bar, 50–300 °C) and desorption (250–350 °C, 50 mbar–1 bar). The combined effects of Pd and Ni additions prove particularly useful in providing superior kinetics at very modest absorption conditions and excellent cyclic stability. These data are compared with those of nanocrystalline MgH_2 powders, obtained by intensive milling in argon atmosphere.
© 2005 Elsevier B.V. All rights reserved.

Keywords: Hydrogen storage materials; High-energy ball milling; Scanning electron microscopy; X-ray diffraction; Nanocrystalline materials

1. Introduction

Magnesium hydride has recently attracted much attention as a potential high density hydrogen storage material. However, due to its poor reaction kinetics and high thermodynamic stability, its applications have been limited. On the other hand, nickel and palladium are well known to be hydride forming metals, which exhibit fast reaction rates and extremely low hydride stability [1]. Several attempts were made [2–4] to obtain Mg–Ni and/or Mg–Pd compounds especially for low additives concentrations, using mainly the ball milling technique. In this work, the hydrogen storage characteristics of induction melted and then reactively milled Mg–1 wt.% Ni–0.2 wt.% Pd are analysed and compared with ball milled MgH_2.

2. Experimental

Despite the large differences in melting points and the high vapour pressure of magnesium, the alloy Mg–1 wt.% Ni–0.2 wt.% Pd was successfully prepared via induction melting starting from the elements. The alloy ingot was filed and reactively milled in a planetary mill (Fritsch P7) using stainless steel vial and balls, in H_2 atmosphere (7 bar) up to 200 h; the total amount of powder was 3.5 g and the ball-to-powder weight ratio was 10:1. As a comparison, a sample of nanocrystalline MgH_2 (nc-MgH_2) was obtained by intensive milling for 80 h, 10 g of magnesium hydride powders (95+%, Goldschmidt GmbH, Germany) in argon atmosphere using a Retsch planetary mill. The ball-to-powder weight ratio was again 10:1.

The crystal structure evolution of both samples was monitored during milling and after desorption in vacuum at 350 °C using a Philips 1050 diffractometer (Co Kα radiation). Field emission gun scanning electron microscopy (FEGSEM LEO 1530) was used to investigate the powder morphology after milling and after absorption/desorption cycling and, using embedded and polished samples, to study the microstructure after H_2 desorption. Hydrogen absorption and desorption reactions were studied as a function of time, at constant temperature and pressure in a wide parameter range (1–10 bar, 50–300 °C for absorption, 50 mbar–1 bar, 250–350 °C for desorption) using gravimetric analysis

* Corresponding author. Tel.: +49 351 4659 664; fax: +49 351 4659 781.
E-mail address: O.Gutfleisch@ifw-dresden.de (O. Gutfleisch).

0925-8388/$ – see front matter © 2005 Elsevier B.V. All rights reserved.
doi:10.1016/j.jallcom.2004.09.083

(Hiden IGA). Oxygen content analysis was performed with a hot extraction LECO apparatus.

3. Results and discussion

The evolution of X-ray diffraction patterns during reactive milling of Mg–1 wt.% Ni–0.2 wt.% Pd is shown in Fig. 1. The starting alloy is composed mainly of metallic Mg; solubility of Ni and/or Pd in the magnesium lattice is considered to be negligible, since the diffraction peaks match the literature values [5]. Moreover, a small peak at 44.5° is present and cannot be related with pure magnesium metal, nor with Ni or Pd. However, it is present also in the diffraction spectrum of a similarly produced Mg–1 wt.% Ni–0.5 wt.% Pd powder and its intensity can be correlated with the concentration of palladium in the alloy. We attribute this peak to a palladium-magnesium intermetallic compound, possibly Mg_6Pd [6], also considering that no Pd-Ni phases are known [7].

After 18 h of milling, the Mg peaks are broader, the Mg–Pd phase has disappeared and the β-MgH_2 phase is present together with elemental iron resulting from milling tools erosion by the rather ductile starting material. For prolonged milling times, the magnesium phase reacts completely with hydrogen forming β-MgH_2, the concentration of iron increases and after 118 h the metastable γ-MgH_2 phase appears. The X-ray diffraction pattern after 220 h of milling exhibit extremely broadened peaks, indicating that the crystallite size is of the order of 10s of nanometers.

Fig. 2 shows the X-ray diffraction results of the milled nc-MgH_2 sample as a function of milling time. The original powder is composed mainly of MgH_2 and exhibits small traces of pure Mg, in accordance to the producer's data sheets.

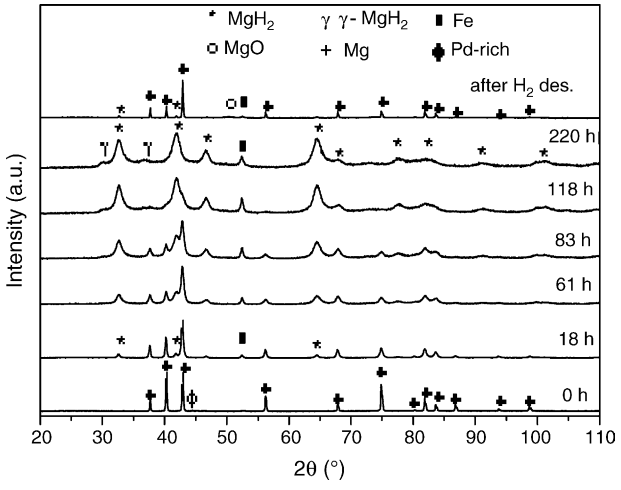

Fig. 1. X-ray diffraction patterns of Mg–1 wt.% Ni–0.2 wt.% Pd produced via induction melting and reactive milling for various durations and after H_2 absorption/desorption cycling, ended with desorption at 350 °C, 50 mbar.

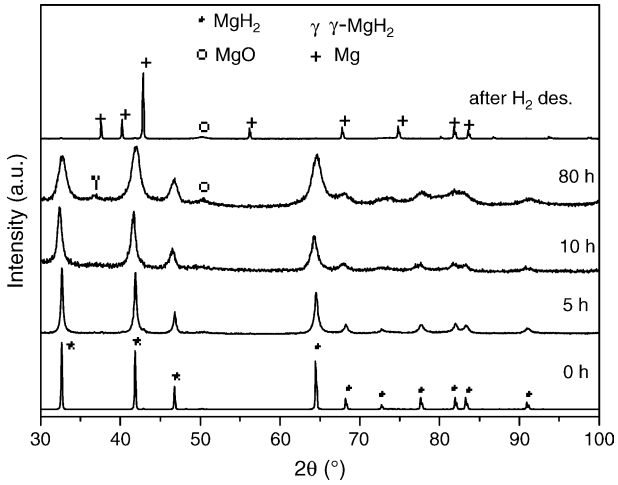

Fig. 2. X-ray diffraction patterns of MgH_2 intensively milled in a planetary mill for various durations and after H_2 absorption/desorption cycling, ended with desorption at 350 °C, 50 mbar.

The peak width increases with the milling time, indicating that grain refinement is taking place and that internal strain is also increasing. A small and extremely broadened peak at 50.2° appears after 20 h of milling and is attributed to the presence of magnesium oxide.

In the as-milled state, both powders are composed of larger agglomerates (20–200 μm) of smaller particles (100 nm–2 μm), as it is evident from the SEM image shown in Fig. 3. The surface of the powders is very irregular, as a result of the repeated fracturing events during the milling process.

The powders obtained after milling have been subjected to three activation cycles (H_2 absorption: 350 °C, 10 bar; H_2 desorption: 300 °C, 50 mbar) and the kinetics were checked to be fully reproducible after the third desorption. All the data presented hereafter are taken on the fully activated samples. Figs. 4 and 5 show the most significant results of isothermal/isobaric experiments on both Mg–1 wt.% Ni–0.2 wt.% Pd and MgH_2 particles at some selected temperatures and

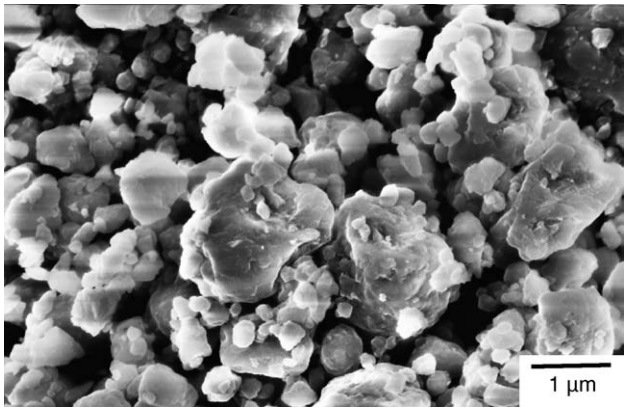

Fig. 3. SEM image of sample Mg–1 wt.% Ni–0.2 wt.% Pd after reactive milling for 220 h taken in the secondary electrons mode.

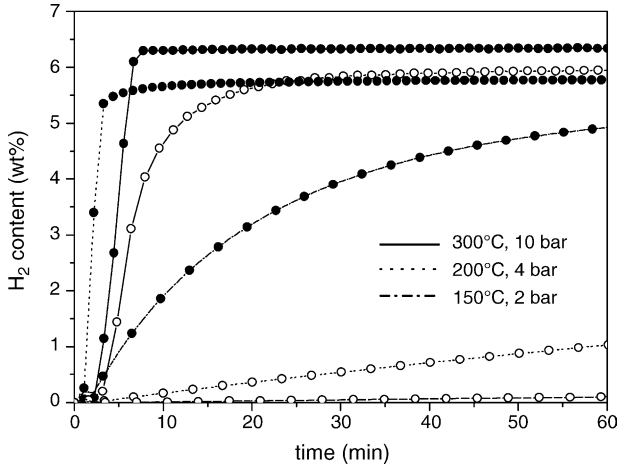

Fig. 4. Results of hydrogen absorption experiments performed on fully activated Mg–1 wt.% Ni–0.2 wt.% Pd (•) and nc-MgH_2 (○) samples at constant temperatures and pressures.

pressures. At 300 °C and 10 bar, the H_2 absorption by Mg–1 wt.%Pd–0.2 wt.%Pd is extremely fast, being completed in less than 5 min, while the reaction kinetics of nc-MgH_2 are slightly slower. The difference between the two samples becomes striking at lower temperatures (Fig. 4): at 200 °C, 4 bar, Mg–1 wt.% Ni–0.2 wt.% Pd can be rehydrided within 5 min, while it takes hours for nc-MgH_2 to complete the hydriding reaction. Even more interesting, at 150 °C the Mg–1 wt.% Ni–0.2 wt.% Pd material can be rehydrided within a reasonable time, while after 3 h the nc-MgH_2 reaction is still at the beginning.

Isothermal-isobaric desorption kinetics are reported in Fig. 5. The desorption reaction appears to be much slower than the absorption one, both for Mg–1 wt.% Ni–0.2 wt.% Pd and for nc-MgH_2, in agreement with literature. However, the former can be fully dehydrided at 285 °C, 50 mbar within 25 min, while it takes hours for the latter to complete the desorption reaction.

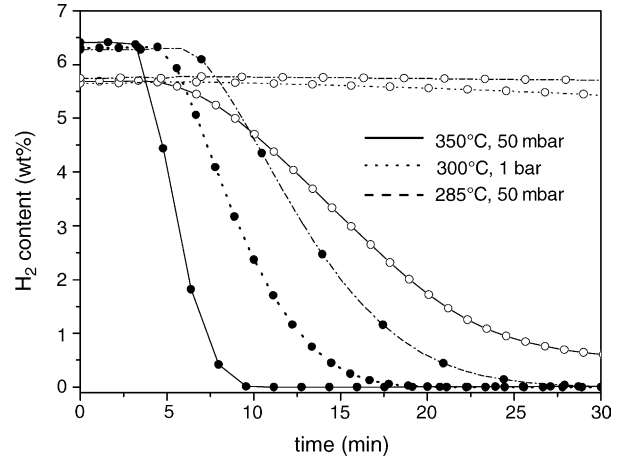

Fig. 5. Results of hydrogen desorption experiments performed on fully activated Mg–1 wt.% Ni–0.2 wt.% Pd (•) and nc-MgH_2 (○) samples at constant temperatures and pressures.

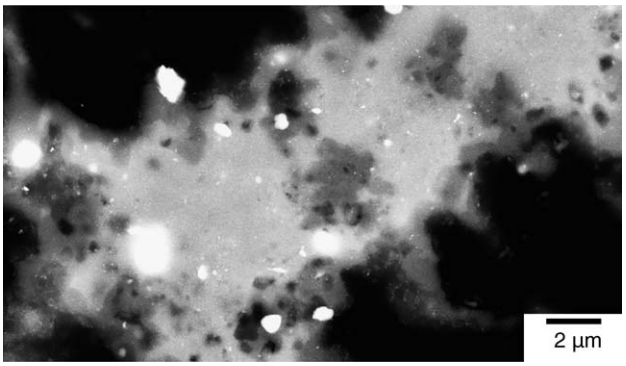

Fig. 6. Backscattered electron SEM image taken on polished Mg–1 wt.% Ni–0.2 wt.% Pd after H_2 cycling, ended with desorption at 350 °C, 50 mbar. The grey region is the Mg matrix, while brighter spots are Pd- and/or Ni-rich precipitates, as well as Fe particles, according to EDX analysis.

In order to characterise the temperature dependence of the reaction rate, hydriding/dehydriding reactions were studied for both samples at constant H_2 pressure (10 bar, 50 mbar respectively) at different temperatures. Following Ref. [8], the reaction rate was estimated taking the hydrogen content at 20 and 80% stage. This approach was preferred to the interpolation with approximated analytical reaction curves [9] because it is model-independent. Using this approach, the activation energy for the Mg–1 wt.% Ni–0.2 wt.% Pd sample was estimated to be 41 kJ/mol for absorption and 110 kJ/mol for the desorption reaction.

X-ray diffraction patterns of the samples taken after H_2 cycling (>50 times) ended with desorption at 350 °C, 50 mbar (Figs. 1 and 2), show that both samples are composed of pure Mg and traces of magnesium oxide. The Mg–1 wt.% Ni–0.2 wt.% Pd sample shows traces of iron and MgH_2, due to incomplete dehydrogenation during the last desorption. The width of Mg Bragg peaks is equal to the instrumental one, indicating that significant grain growth has taken place. SEM studies after hydrogen cycling show that the Mg–1 wt.% Ni–0.2 wt.% Pd powder morphology remains largely unchanged, while the surface of the nc-MgH_2 powder is more regular. The particles are of a more rounded shape and exhibit a tendency to sinter. Backscattered electron images on polished Mg–1 wt.% Ni–0.2 wt.% Pd (Fig. 6) show the presence of Pd and Ni segregations of almost spherical shape, together with Fe particles. The nc-MgH_2 sample shows only small traces of Fe. The Fe concentration is much reduced as compared with the previous sample, in agreement with X-ray diffraction spectra, which is attributed to the much more brittle nature of the MgH_2 starting material.

The overall reversible H_2 storage capacity of Mg–1 wt.% Ni–0.2 wt.% Pd and nc-MgH_2 is 6.3 and 5.8 wt.%, respectively, as shown in Figs. 4 and 5. These data are somewhat lower than the theoretical capacity (7.5 wt.% for the former and 7.6 wt.% for the latter), assuming that Ni and Pd do not absorb a significant amount of H_2 at the operating conditions considered here. Oxygen content of the powders was analysed to be approximately 5 wt.% for both samples, which

would reduce the overall capacity to 6.3 wt.%, in reasonable agreement with the obtained H_2 absorption/desorption data.

As for absorption reaction, the reaction rates at the temperatures reported here are comparable with the best results obtained on Mg-based composites by other groups [8,10,11] using the ball milling technique. The rate dependence on temperature and pressure involves two independent factors, namely the Arrhenius term – which depends on temperature – and the driving force – which is a function of the ratio between operating and equilibrium pressure. This is the reason why the H_2 absorption rate at 300 °C, 10 bar is higher than at 200 °C, 4 bar, opposite to what might be expected. The activation energies obtained for the H_2 absorption/desorption reactions are in agreement with what has been obtained for similarly performing materials [8].

The excellent performance of the Mg–1 wt.% Ni–0.2 wt.% Pd material can be explained taking into account the effect of transition metal additives on the Mg–H_2 reaction. Ni and Pd particles dispersed on the surface and inside the Mg matrix (Fig. 6) act as catalysts for the H_2 molecule dissociation/recombination [1], overcoming the low reactivity of the Mg surface. With respect to this, the finely dispersed Fe particles could also play a beneficial role, since the heat of hydrogen chemisorption on Ni and Fe surface is almost equal [1]. Moreover, thanks to their enhanced reactivity towards hydrogen, Pd and Ni particles are excellent fast nucleation sites both during absorption and desorption processes.

Even if the nanocrystallinity of the powder is largely lost during the H_2 treatment, the reaction kinetics remain excellent over more than 50 cycles. This observation implies that the crystallinity of the material does not play such a significant role, when compared with the presence of finely dispersed transition metal particles and with the morphology of particles.

4. Summary

A Mg–1 wt.% Ni–0.2 wt.% Pd alloy was successfully produced via induction melting and then reactively milled. This process results in nanocrystalline, high surface area powders with finely dispersed Ni- and/or Pd-rich particles. This material exhibits excellent hydrogen absorption/desorption kinetics, which are stable upon cycling and far superior to nanocrystalline magnesium hydride.

Acknowledgements

Technical cooperation of Dr. Gruner in performing oxygen analysis is gratefully acknowledged. The work was supported by the EU project FUCHSIA. A patent has been filed.

References

[1] W.M. Mueller, J.P. Blackledge, G.P. Libowitz, Metal Hydrides, Academic Press, New York, London, 1968, p. 629.
[2] S. Orimo, H. Fujii, Appl. Phys. A 72 (2001) 167.
[3] O. Gutfleisch, N. Schlorke-de Boer, N. Ismail, M. Herrich, A. Walton, J. Speight, I.R. Harris, A.S. Pratt, A. Züttel, J. Alloys Compd. 356–357 (2003) 598.
[4] A. Zaluska, L. Zaluski, J.O. Ström-Olsen, J. Alloys Compd. 298 (1999) 197.
[5] Powder Diffraction File, JCPDS card # 89–4894.
[6] Powder Diffraction File, JCPDS card # 25–1084.
[7] T.B. Massalski (Ed.), Binary Alloys Phase Diagrams, vol. II, ASM International, 1990.
[8] G. Barkhordarian, T. Klassen, R. Borrmann, J. Alloys Compd. 364 (2004) 242.
[9] G. Liang, J. Huot, S. Boily, R. Schulz, J. Alloys Compd. 305 (2000) 239.
[10] G. Liang, J. Huot, S. Boily, A. Van Neste, R. Schulz, J. Alloys Compd. 291 (1999) 295.
[11] K.J. Gross, P. Spatz, A. Züttel, L. Schlapbach, J. Alloys Compd. 261 (1997) 276.